Dynamics and Cloud Microphysics of the Rainbands in an Occluded Frontal System[1]

ROBERT A. HOUZE, JR., JOHN D. LOCATELLI AND PETER V. HOBBS

Department of Atmospheric Sciences, University of Washington, Seattle 98195

(Manuscript received 13 April 1976, in revised form 15 June 1976)

ABSTRACT

The dynamics and cloud microphysics of four rainbands in an occluded frontal system were examined. Aircraft, radar, raingage, and serial rawinsonde observations were obtained in addition to standard satellite and synoptic data. Two of the rainbands occurred in the leading portion of the frontal cloud shield and were oriented parallel to the warm front of the system. The other two bands occurred in the trailing portion of the cloud shield and had cold frontal orientations. Mesoscale pressure features were parallel to the rainbands, except in mountainous areas. Computed air motions showed that the rainbands were supplied with moist air flowing into the rainband region from the south to south-southwest at low levels (below 800 mb). This air was swept abruptly upward in the rainbands just ahead of the cold air mass approaching from the west. Cumulus-scale convection in a layer between 4 and 5 km in clouds associated with these rainbands appeared to enhance the growth the ice particles. However, the ice crystal habits in these regions did not appear to be affected by the presence of the convection. As the ice particles settled below the convective layer, they grew first by vapor deposition and then, just above the melting layer, they began to grow by riming or aggregation. High ice particle concentrations were measured beneath the convective layer. Below the melting layer, very little precipitation growth took place in the rainbands, and in the two warm frontal bands, considerable evaporation of raindrops occurred below the melting layer.

1. Introduction

Recent studies of mid-latitude precipitation systems have shown that mesoscale rainbands[2] (5 to 100 km in width and 100's of km in length) are a characteristic feature of extratropical cyclones (Browning, 1974; Harrold and Austin, 1974; Houze *et al.*, 1976). These studies have provided insight into the structure and dynamics of extratropical cyclones. However, if the rainbands in mid-latitude cyclones are to be understood fully, the relationships between cloud microphysical processes and larger scale air motions associated with the bands must be established. Toward this end, a wide variety of field measurements must be brought to bear on extratropical storms.

As part of the CYCLES (CYCLonic Extratropical Storms) PROJECT at the University of Washington, we have collected aircraft, radar, raingage and serial rawinsonde data simultaneously in order to investigate frontal cyclones on scales ranging from the synoptic down to individual cloud particles. This paper describes an intensive study of CYCLES data for four rainbands in one occluded frontal system. We have examined the dynamics and cloud microphysics of these bands from six points of view: (i) the relationship of the bands to the fronts, (ii) the relationship of the bands to the surface pressure field, (iii) air motions associated with the bands, (iv) sources and sinks of moisture for the bands, (v) the role of cumulus-scale convection in the bands, and (vi) the modes of growth of precipitation particles in the bands.

2. Location and period of observations

The rainbands to be described were located within the second of three occluded frontal systems which passed over the area of observations shown in Fig. 1 during the period 1400 PST 19 December 1973 through 1700 PST 21 December 1973. Observations were maintained throughout this period, and aircraft measurements in the rainbands to be described were obtained from 0938 to 1249 on 20 December 1973. The flight path is shown in Fig. 1.

3. Types of data

a. Rawinsonde data

Rawinsondes were launched at intervals of 2–3 h from the University of Washington in Seattle (Fig. 1).

[1] Contribution No. 380, Department of Atmospheric Sciences, University of Washington.

[2] Although in the past the term *rainband* has generally been used to describe a horizontal area of rainfall, in this paper we extend the term to include the complete three-dimensional cloud and precipitation structure (solid and liquid) associated with the rainband. The term rainband will often be shortened to *band*.

These serial soundings were used to construct cross sections through the frontal systems passing over the area. The horizontal wind data from the soundings were used to compute the vertical velocity ω ($\equiv dp/dt$, where p is pressure and t is time) using the two-dimensional form of the mass continuity equation

$$\frac{\partial \omega}{\partial p} = -\frac{\partial u}{\partial x}, \tag{1}$$

where x is the horizontal coordinate normal to a front and u the wind component in the x direction.

Attempts to compute ω from the conservation of wet-bulb potential temperature (θ_w), or on the assumption of thermal wind balance in the equation for the local time-rate of temperature change, were unsuccessful because of the predominance of near-zero vertical gradients of θ_w, which appear in the denominators of the equations for ω in both of these methods.

b. Raingage data

High-resolution tipping-bucket raingages with resolutions of ~0.04 mm of rain per tip (time resolution in moderate rain about 15 s) were operated by the University of Washington at the locations shown in Fig. 1. Lower resolution gages were operated by the National Weather Service; these were weighing bucket gages from which rainfall amounts of ~0.5 mm could be resolved over time periods of about 7 min.

c. Radars

Two radars were operated at the University of Washington (UW). One was a weather surveillance radar (wavelength 3.2 cm, beamwidth 1.5°, peak power 250 kW) which provided approximately horizontal coverage within a 90 km radius of the radar (Fig. 1). The PPI displays for this radar were recorded by time-lapse photography as the displays were cycled through a series of five gain settings. In this way, intense echo cores (shown on minimum-gain displays) as well as widespread light rain areas (shown on high-gain displays) could be identified and tracked.

The second radar was a vertically-pointing pulsed Doppler radar (wavelength 3.2 cm, beamwidth 0.8°, peak power 7 kW) which detected precipitation and measured the spectrum of fallspeeds of precipitation particles at ten levels in the vertical (Weiss and Hobbs, 1975). A complete set of ten velocity spectra was obtained at intervals of 50 s throughout the study, and these were displayed in real time on a cathode ray storage scope. The spectra were recorded both digitally and by photographing the storage scope displays.

d. Aircraft measurements

The University of Washington's B-23 research aircraft was used in this study. Parameters measured aboard the B-23 include cloud liquid water content, cloud droplet sizes and concentrations, ice particle sizes, types and concentrations, air turbulence, temperature and dew point. The position of the aircraft is continually recorded in real time on a map of the area with the aid of an $x-y$ plotter. Cloud photography and visual observations are also made from the aircraft. A detailed listing of the cloud physics capabilities of the B-23 can be found in Hobbs *et al.* (1975).

e. Other data

Satellite photographs, conventional maps and microbarograph traces were obtained from the National Environmental Satellite Service and the National Weather Service.

4. Synoptic situation

The first of the three occluded frontal systems which we observed is shown in Figs. 2a and 2b as it was approaching the Washington coastline on 19 December 1973. The second occluded system passed over Washington on 20 December (Figs. 2c and 2d) and the third one, which formed when the "comma cloud" shown in Fig. 2c merged with the frontal wave to the east, moved over the Pacific Northwest on 21 December (Figs. 2e and 2f). These three frontal systems were embedded in a southwesterly upper-level flow between a 500 mb ridge over the western United States (Fig. 2b) and a 500 mb trough to the west, which moved gradually from the Gulf of Alaska region (Fig. 2b) toward the western coast of the United States (Fig. 2f).

Vertical cross sections through the three frontal systems which passed over UW's rawinsonde site on 19–21 December are shown in Fig. 3. None of these systems exhibited any discernible frontal structure below the 850 mb level in the cross sections. Above 850 mb, however, fronts were well defined. (The cold front shown at the surface on 21 December occurred after the passage of the third frontal system. This lower level front coincided with the passage of a line of convective showers and thus may have been a convectively induced phenomenon.)

The frontal system which moved over UW on 19 December was characterized first by the passage of a well-defined cold front located between 800 and 600 mb at 1730 PST in Fig. 3. This cold front was followed by a second cold front[3] located between 600 and 470 mb at 1900 PST on 19 December. This second cold front was connected at its lower end with a warm occlusion which extended downward from 600 mb at 1900 to 850 mb at 2300.

The leading portion of the second frontal system, which moved over UW on 20 December, contained a warm front extending downward from 630 mb at 0500

[3] In our terminology, a single frontal *system* may consist of several individual *fronts* arranged in various configurations.

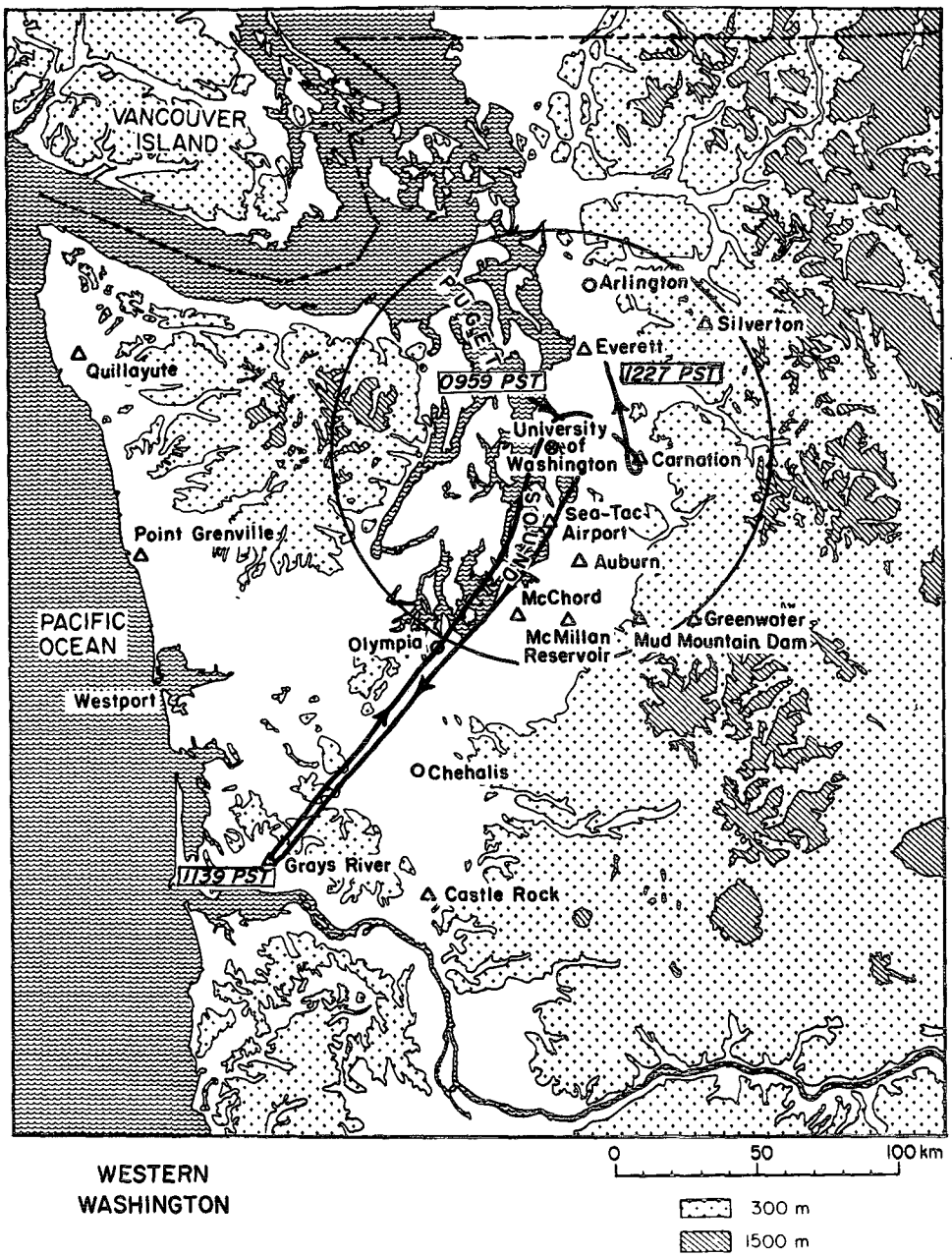

FIG. 1. CYCLES data network on 19–21 December 1973. Arrow shows aircraft flight path from 0959 to 2127 PST 20 December. Symbols are for high-resolution raingage sites (○), low-resolution raingage sites (△), barograph locations (●), and the University of Washington (⊗) where radar, rawinsonde, continuous pressure and wind measurements and high-resolution raingage data were obtained.

to 740 mb at 1000 on the 20th (Fig. 3). The warm front was followed by a surge of cold air bounded at about 1100 in Fig. 3 by two cold fronts which were separated at the 670 mb level, with the upper cold front slightly ahead of the lower one. This split in the cold fronts aloft is consistent with the wet-bulb potential temperature pattern seen in Fig. 3c, and with the vertically-pointing Doppler radar data which provided a continuous record of the 0°C isotherm (as evidenced by a discontinuity in precipitation particle fallspeed due to melting; see further discussion in Section 9).

The third frontal system, which passed over UW

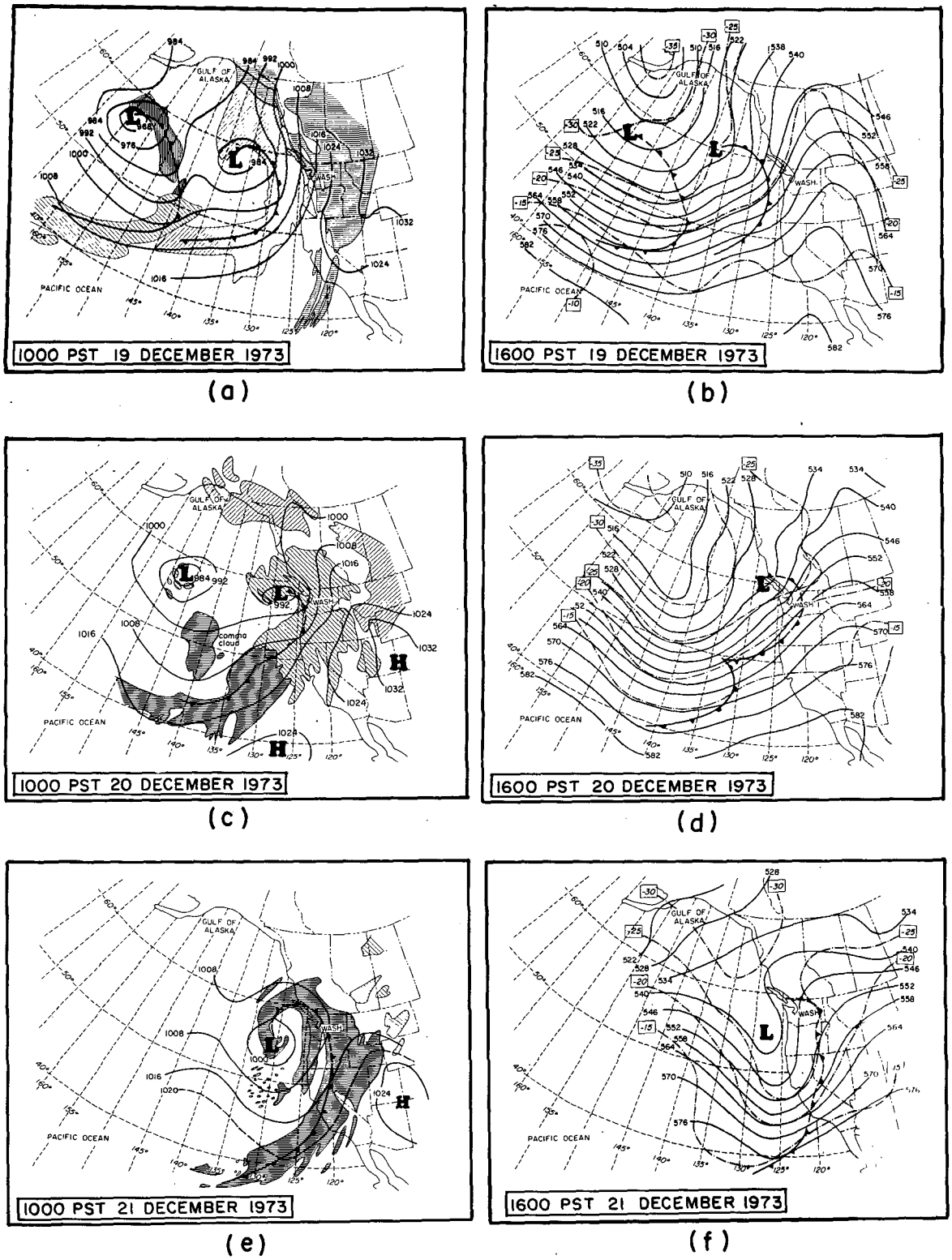

FIG. 2. Synoptic map sequence for 19–21 December 1973. Surface maps (a, c and e) show isobars (mb), low (L) and high (H) pressure centers and fronts. The satellite cloud patterns (traced from NOAA 2 infrared images) for a specific frontal system may be tracked in time by following the same style of shading from one surface map to the next. Upper air maps (b, d and f) show 500 mb height contours (solid lines, dam) and isotherms (dash-dotted lines, °C). Surface fronts and pressure centers are superimposed on 500 mb maps.

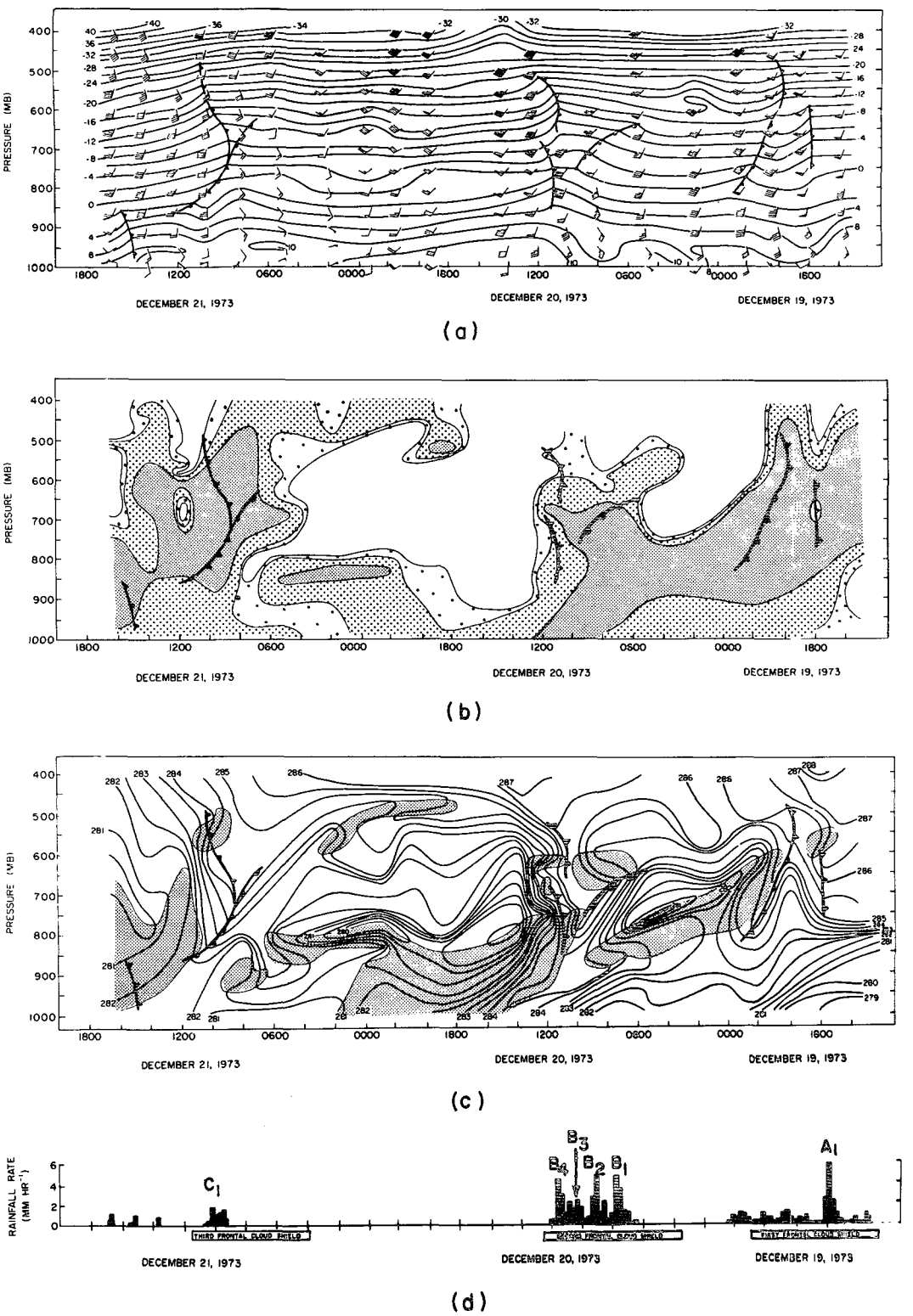

FIG. 3. Rawinsonde and raingage data obtained at the University of Washington, 19–21 December 1973. (a) Cross section showing fronts, isotherms (°C) and winds (kt). (b) Cross section showing fronts and relative humidity with respect to liquid water. Contours of relative humidity are for 30, 50, 70 and 90% with the darkest shading indicating values >90% and the unshaded regions indicating values <30%. (c) Cross section showing fronts and isotherms of wet-bulb potential temperature (θ_w, K). Regions of potential instability are indicated by shading. (d) Raingage trace with rainbands indicated by A_1, B_1–B_4 and C_1.

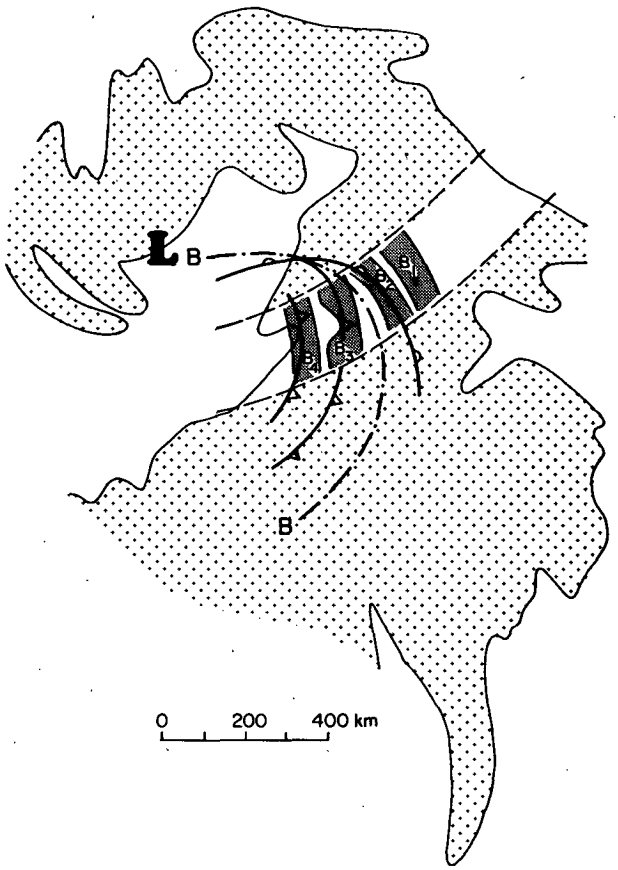

FIG. 4. Relationship of rainbands B_1–B_4 to satellite cloud pattern and synoptic features. Specific features indicated are fronts at the 720 mb level, surface low pressure center (L), and surface pressure trough (B). Open swath between dashed lines shows portion of cloud shield in which observations were obtained.

between 0400 and 1200 on 21 December, was a classical warm occulsion with the cold front advancing over the warm front (Fig. 3).

The fragmented nature of the first two frontal systems (19 and 20 December in Fig. 3), which had cold air arriving in multiple surges aloft, appears to be a commonly observed feature of occluded frontal systems, as described by Kreitzberg (1964), Elliott and Hovind (1965), Kreitzberg and Brown (1970), Browning *et al.* (1973) and Hobbs *et al.* (1975).

5. Relationship of rainbands to fronts

The three frontal cloud systems which passed over UW on 19, 20 and 21 December, respectively, each contained mesoscale rainbands, which are denoted A_1, B_1–B_4 and C_1 in Fig. 3d. In the remainder of this paper, we focus attention on B_1–B_4, the four rainbands embedded in the frontal system of 20 December.

The times that rainbands B_1–B_4 passed over each raingage station shown in Fig. 1 were noted, and the horizontal positions and motions of the bands were then inferred from these times, cross-checking the results against echo patterns from the UW weather surveillance radar. A description of this analysis technique and of the horizontal structure and motion of rainbands B_1-B_4 is given in a separate paper (Houze *et al.*, 1976). We note here only that bands B_1 and B_2, which occurred in the leading portion of the 20 December frontal system, had a warm-frontal orientation (northwest to southeast) as they moved across western Washington, while B_3 and B_4, in the trailing portion of the cloud system, had a north–south (or cold-frontal) orientation. This result would be expected from Fig. 3, since the passage of B_1 and B_2 coincided with the passage of the upper-air warm front on 20 December, while the later bands (B_3 and B_4) coincided with the two upper-air cold fronts on this day. The relationship of the rainbands to the fronts on 20 December is summarized in Fig. 4.

6. Rainbands in relation to surface pressure features

Properties of the surface pressure field on 20 December 1973 are indicated by the barograph traces shown in Fig. 5. Features A and C were mesoscale pressure perturbations superimposed on the general fall and rise of pressure associated with the large-scale trough B. Feature A marked *the end of a period of rapidly falling pressure*, after which the pressure fell less rapidly, leveled-off temporarily, or showed a temporary rise in pressure. Feature C was *the beginning of a period of rapidly rising pressure*, which followed a period of less-rapidly rising pressure, a period of constant pressure,

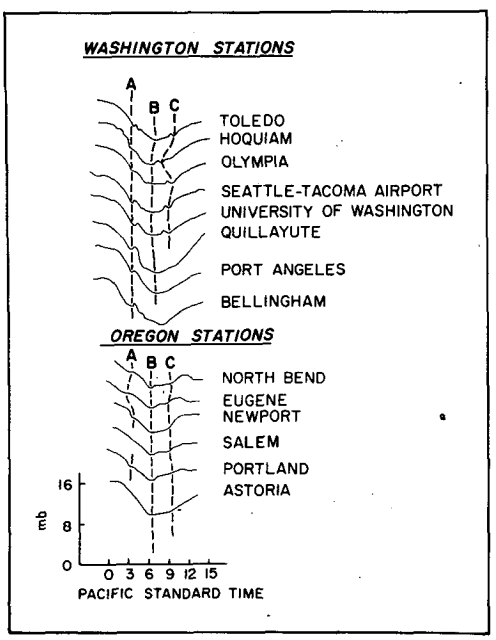

FIG. 5. Barograph traces for Washington and Oregon for 20 December 1973. Features A, B and C are discussed in text.

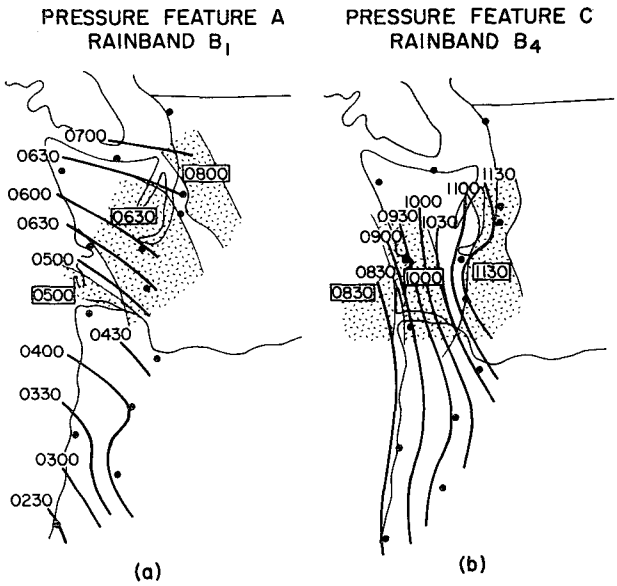

FIG. 6. Isochrones of pressure features A and C and successive positions of rainbands B_1–B_4 on 20 December 1973. Times for isochrones and rainbands (shaded areas) are in Pacific Standard Time. Dots show barograph locations.

or a temporary fall in pressure. At most of the Washington sites included in Fig. 5, feature A was immediately followed by a short-lived but well-defined peak in the pressure field, while C was immediately preceded by a pronounced pressure peak.

The movement of A and C over western Oregon and Washington is shown in Fig. 6 with successive positions of rainbands B_1 and B_4 superimposed on the pressure line positions. The earlier pressure feature A and rainband B_1 (Fig. 6a) had northwest–southeast orientations, whereas the later pressure line C and rainband B_4 (Fig. 6b) had north–south orientations. Thus, mesoscale features in the pressure field, as well as the precipitation field, were oriented parallel to the warm front in the leading (or eastern) part of the storm, while those which came later (in the western part of the storm) had a cold-frontal orientation.

The similar orientations of the rainbands and pressure lines were most noticeable when they first moved onshore from the Pacific Ocean. In Fig. 6a it can be seen that as the features moved inland, the pressure feature rotated toward an almost east–west orientation by 0700, while the rainband tended toward a more north–south orientation. The change in orientation of the rainband, however, occurred as it approached the meridionally oriented Cascade Range in central Washington and was probably due to orographic modification of the rainfall pattern. In the absence of orographic influences, the rainband and pressure line might have remained parallel.

The positions and motions of various features embedded within the frontal system of 20 December are summarized in Fig. 7. Since the total lengths of the rainbands and pressure lines were not observed, only the components of motion normal to these features could be shown in the figure. It is evident from Fig. 7 that the warm-frontal rainbands B_1 and B_2 and the pressure features A and B moved somewhat faster than the frontal cloud shield; however, several tens of hours would have been required for these features to move from one edge of the cloud shield to the other and the change in structure of the cloud system due to this relative motion was thus rather gradual. The vectors shown inside of the rainbands B_1–B_4 in Fig. 7 indicate the average motion of small mesoscale precipitation areas situated within the bands. These small elements, described in the paper by Houze *et al.* (1976), were the cores of heaviest rainfall within the rainbands. They were 10's to 100's of km^2 in area and moved with the winds between 850 and 700 mb.

7. Air motions

Vertical velocities computed by integrating Eq. (1) were combined with the horizontal winds normal to the fronts to obtain a two-dimensional, vertical circulation pattern for the frontal system containing rainbands B_1–B_4 (Fig. 8). The horizontal velocity of the frontal

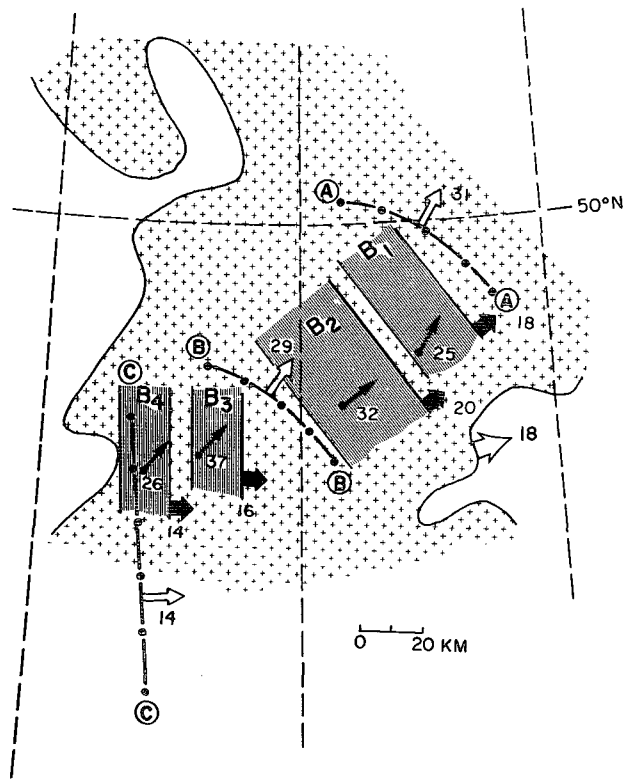

FIG. 7. Composite of the storm system of 20 December 1973 showing positions and velocities (m s^{-1}) of the cloud shield within which were located pressure features (A, B and C), rainbands (B_1–B_4) and small-scale precipitation areas (dots) within the bands.

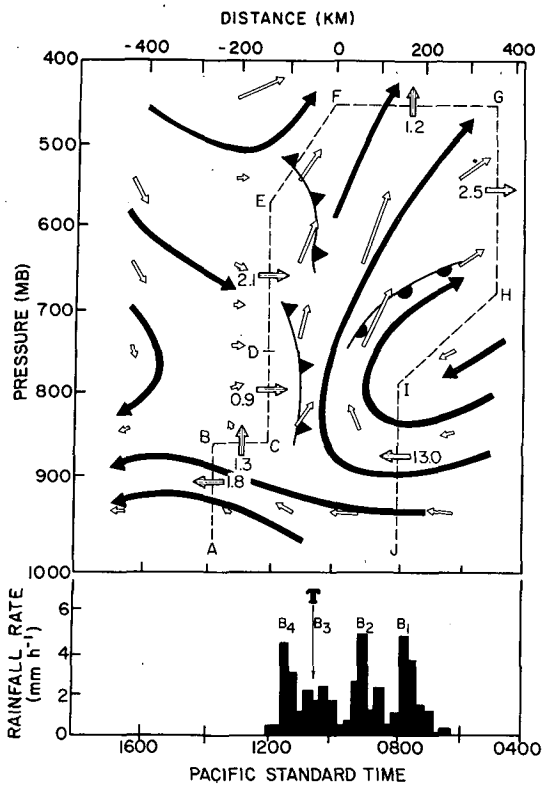

FIG. 8. Two-dimensional airflow in the frontal system of 20 December 1973. Distance scale at top of diagram was obtained by converting time to space on the basis of observed frontal velocities. Streamlines relative to front are shown by heavy arrows. Small white arrows indicate the displacement of a parcel of air in 1 h at the computed velocity applying at its origin (vertical component in mb, horizontal component in km). Dashed line surrounds region of upward motion associated with frontal clouds and rainbands (B_1–B_4). Striped arrows crossing dashed line show fluxes of water vapor (with numbers adjacent to arrows indicating magnitudes of fluxes in units of 10^4 g s^{-1} m^{-1}) across boundaries of lifting region. Letters A–J mark points referred to in text. Letter T marks time of surface trough passage.

system itself has been subtracted from the airflow pattern to represent the flow relative to the system. In the integration of Eq. (1), $\partial u/\partial x$ was computed over horizontal increments (Δx) which were determined by converting the time increments between soundings to distances based on the speed of the frontal system. The horizontal wind component u in (1) was taken in a plane normal to the warm front to the right of 1000 PST in Fig. 8 and in a plane normal to the cold fronts to the left of 1000 PST. The two planes intersect at 1000 at an angle of 137°, and thus together approximate a single slightly curved plane cutting both the cold and warm fronts at right angles. Theoretically, the streamlines in Fig. 8 should show a kink at the intersection of the two planes; however, the kink is so slight that it is imperceptible from the data and has been smoothed over in the analysis.

The computed flow pattern in Fig. 8 is in good agreement with other data. The region of maximum upward motion in the lower troposphere is centered on the time of the surface trough passage (T in Fig. 8), when the maximum low-level convergence would be expected. The computed upward motion region also coincides exactly with the periods of precipitation and satellite-observed cloudiness at the rawinsonde site. The airflow pattern shown in Fig. 8 is remarkably similar to frontal airflow patterns obtained in previous investigations of Pacific occlusions (Elliott and Hovind, 1965; Hobbs *et al.*, 1975).

8. Sources and sinks of moisture

The computed flow of water vapor through the region of upward motion (seen in Fig. 8) shows that the flow of water vapor into the lifting region was exceeding the outflow. The resulting moisture accumulation would have resulted in a rainfall rate of 0.9 mm h^{-1} if the accumulating vapor was being converted to precipitation distributed at a steady rate uniformly over the 350 km wide region containing rainbands B_1–B_4. The average rainfall rate actually observed in the region containing the bands was 1.5 mm h^{-1}, which agrees with the computed rate well within the noise level of the data.

From Fig. 8, it is evident that the primary source of moisture for the frontal clouds was the low-level flow through boundary IJ below the warm front. There is no apparent way that the precipitation in this frontal system could have been supplied by the small horizontal influxes of moisture across the western boundary CDE in Fig. 8. Instead, the precipitating clouds, which comprised the rainbands B_1–B_4, were fed directly from surface layers, with air originating below the 800 mb level.

The origin of the moist air feeding rainbands B_1–B_4 was investigated by estimating the three-dimensional trajectories of the air flowing through the cross section of Fig. 8. We identified four air parcels in the cross section plane and displaced them backward in time (in 1 h steps) according to the computed vertical velocity field indicated in Fig. 8 and the observed horizontal winds shown in Fig. 3a. It was assumed that the airflow in the plane of the cross section of Fig. 8 applied everywhere along a 600 km length of the frontal system. The computed trajectories are shown in Fig. 9. In Fig. 9a the frontal motion has been subtracted from the trajectories to show the flow relative to the fronts, while in Fig. 9b the trajectories are shown in relation to the earth.

From the geographical frame of reference in Fig. 9b, it is evident that the moisture influx along trajectories W, X and Y originated south to south-southwest of the lifting zone with the moist air moving toward the front in a relative sense at low levels and beginning to rise only as it was overtaken by the approaching frontal system. This trajectory pattern is very similar to that observed by Hobbs *et al.* (1975), who further showed

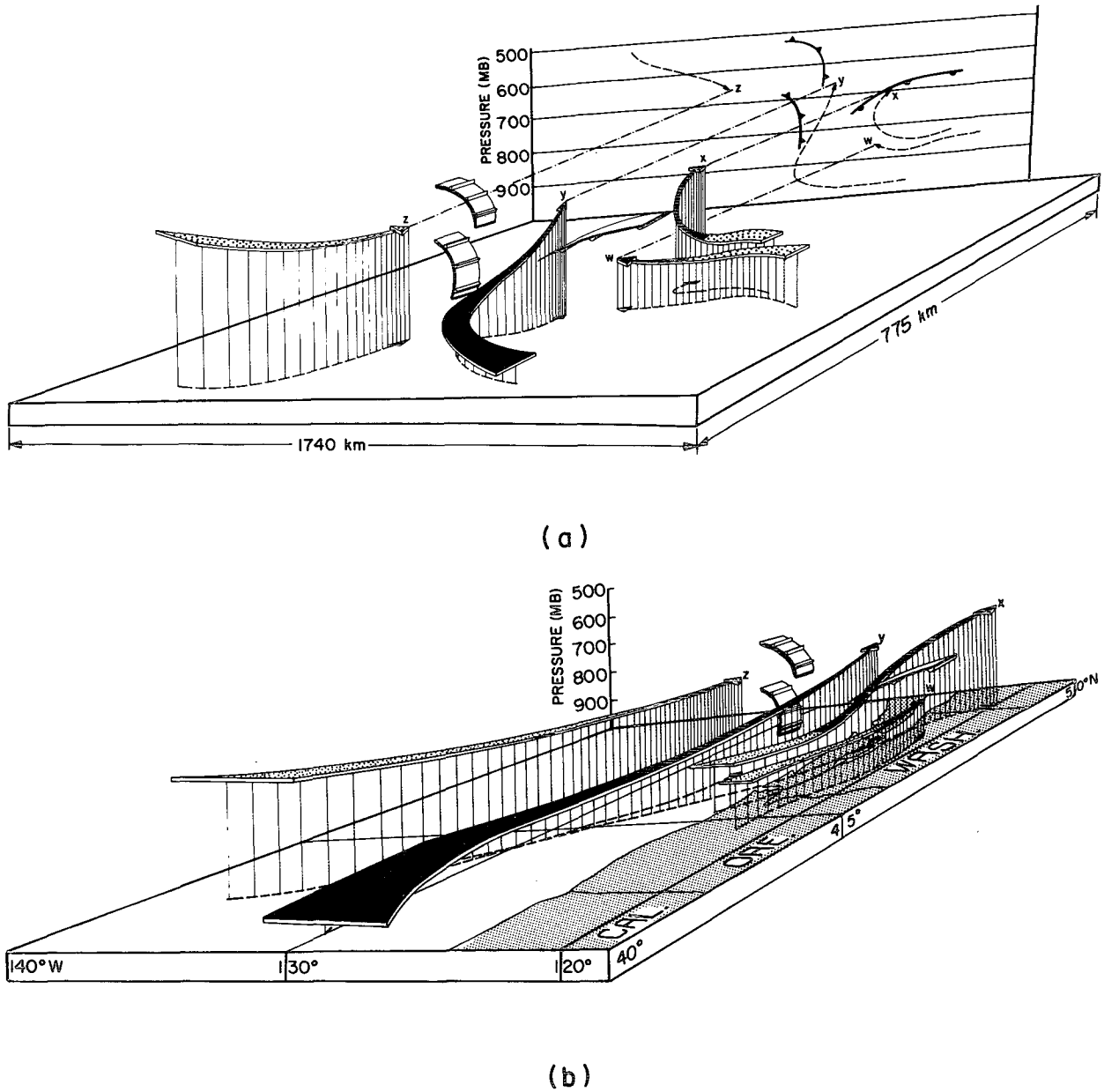

FIG. 9. Three-dimensional trajectories for frontal system of 20 December 1973. Trajectories all begin at 0300 PST and end at 1000 PST. Upward moving portions of trajectories are indicated by solid black shading. Trajectories relative to fronts are shown in (a). The background of (a) shows the two-dimensional projections of trajectories W, X, Y and Z in a format similar to that of Fig. 8. Trajectories relative to the earth are shown in (b). Fronts shown are for 1000 PST.

how such an airflow can be disrupted as it moves over a north–south oriented mountain range.

The southerly trajectories of moist air (W, X and Y in Fig. 9b) suggest that the rainbands in our frontal systems were being fed with generally maritime tropical air. This may explain the potentially unstable stratification in the air above the warm front seen in Fig. 3c, since maritime tropical air typically has a minimum of θ_w in the low to middle troposphere.

9. Growth of precipitation particles and the role of cumulus-scale convection in the rainbands

a. Melting layer

A time-height cross section of average particle fallspeeds, obtained by averaging the vertically pointing Doppler radar data obtained during the passage of rainbands B_1–B_4 over 10 min periods, is shown in Fig. 10. A very prominent feature in this diagram is the

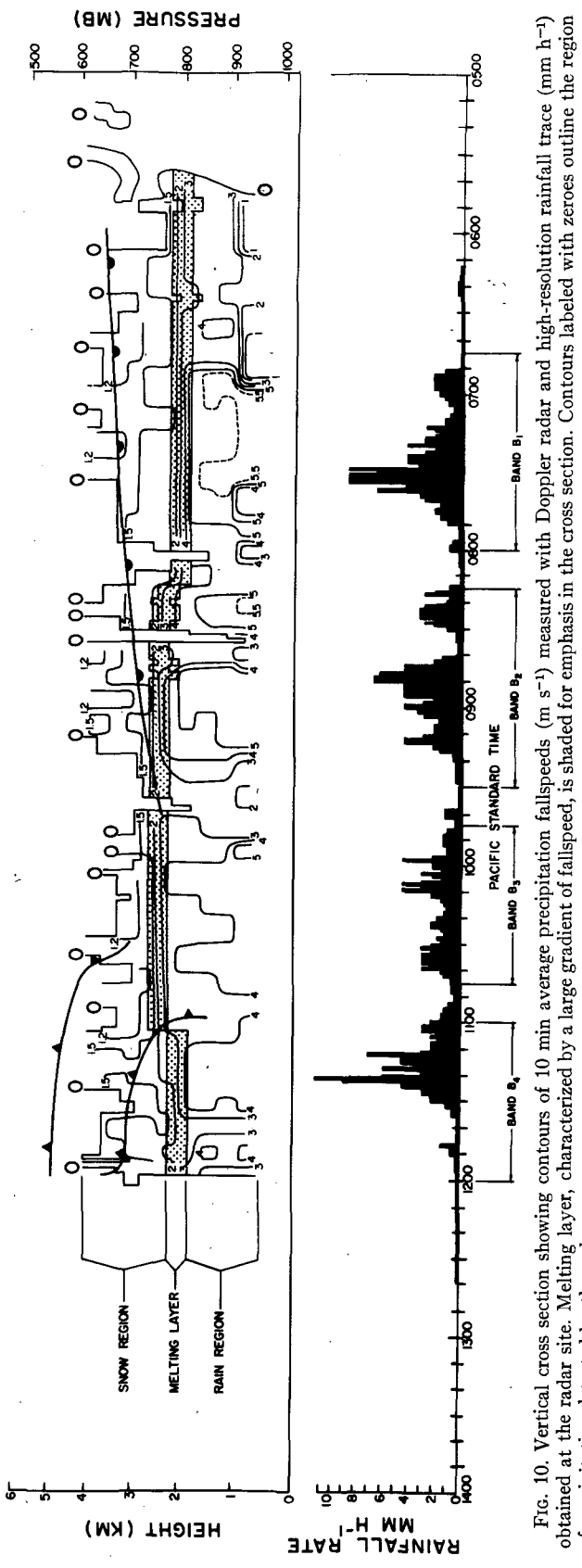

FIG. 10. Vertical cross section showing contours of 10 min average precipitation fallspeeds (m s^{-1}) measured with Doppler radar and high-resolution rainfall trace (mm h^{-1}) obtained at the radar site. Melting layer, characterized by a large gradient of fallspeed, is shaded for emphasis in the cross section. Contours labeled with zeroes outline the region of precipitation detected by the radar.

melting layer, which is indicated by a rapid downward increase in the magnitude of precipitation fallspeeds. The melting layer was consistent with the isotherm pattern indicated by rawinsondes (Fig. 3), and because the radar data were obtained continuously while the rawinsondes were available only every 2–3 h, the radar melting level "isotherm" was particularly helpful in locating the warm front and the lower cold front shown in Figs. 3 and 10.

Above the melting layer, in the "snow region" of Fig. 10, ice particle fallspeeds were generally between 1.0 and 1.5 m s^{-1}. (Mean fallspeeds much less than 1 m s^{-1} were not detected.) Below the melting layer, in the "rain region," the mean fallspeeds of raindrops ranged from 4 to 6 m s^{-1}.

b. Particle growth and evaporation below the melting layer

Very little particle growth (indicated by increasing fallspeeds with decreasing height in Fig. 10) was observed below the melting layer in any of the rainbands. Moreover, a considerable amount of evaporation (indicated by fallspeeds decreasing toward the ground) occurred at the edges of bands B_1 and B_2.[4] Evidently, these two bands, located on the eastern side of the frontal system, were being eroded by the intrusion of low-level unsaturated air.

c. Particle growth above the melting layer

Precipitation particle growth above the melting layer is best indicated by Figs. 11 and 12 which are expanded time cross sections showing rainbands B_1 and B_4.

Weiss and Hobbs (1975) have shown that ice particle growth modes can be related to the vertical gradient of the mean particle fallspeed. A small gradient ($\lesssim 10^{-4}$ s^{-1} in magnitude) is associated with growth by deposition from the vapor phase, while larger gradients are associated with growth by collection processes (either riming or aggregation). Applying these ideas to Figs. 11 and 12, we conclude that the region above about 2.8 km, which was characterized primarily by vertically oriented isotachs of fallspeed, was dominated by depositional growth. Just below 2.8 km, but above the top of the melting layer, the fallspeed isotachs in Figs. 11 and 12 are horizontally oriented and the larger vertical gradient of fallspeed ($\sim 8\times 10^{-4}$ s^{-1} on average) indicates that the particles were growing by riming or aggregation in this region.

d. Cumulus-scale convection

In Section 6 it was noted that rainbands B_1–B_4 contained small-scale cores of heavy rainfall ranging from

[4] The distribution of fallspeeds with height below the melting layer is not likely to be affected by vertical air motions since the terminal fallspeeds of the raindrops are more than an order of magnitude greater than the vertical air velocities in that region.

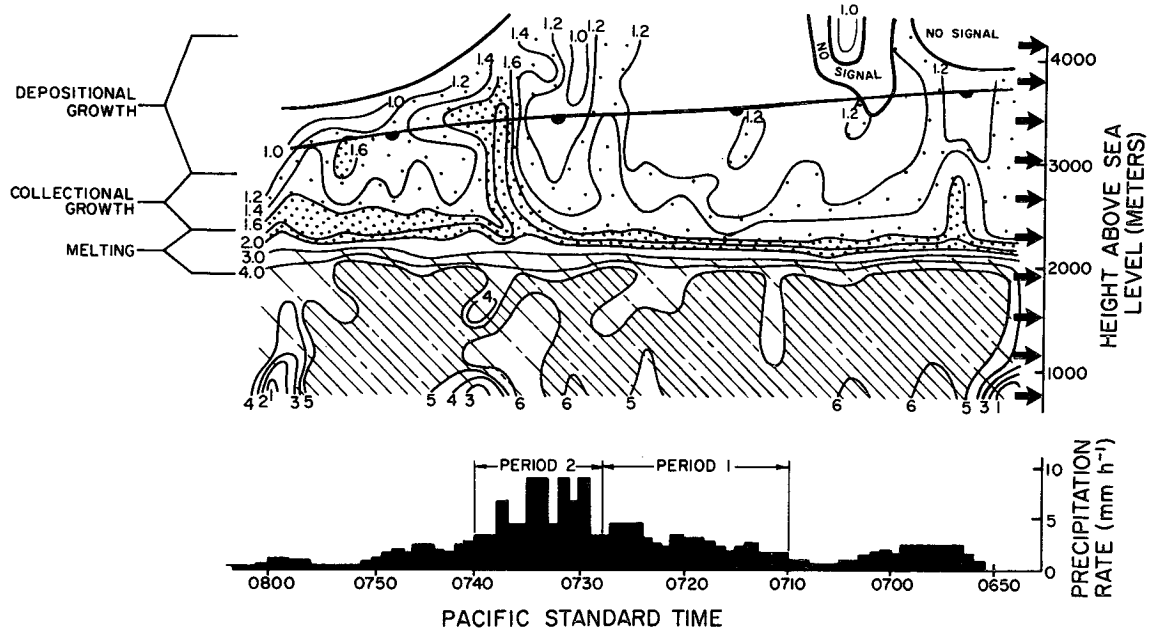

FIG. 11. Vertical cross section showing contours of 3 min average precipitation fallspeeds (m s^{-1}) measured with Doppler radar during the passage of rainband B_1. High-resolution rainfall trace obtained at the radar site is also shown.

1's to 10's of km in horizontal dimension. The track of one such small-scale rain area (~15 km in dimension) located in band B_1 is shown in Fig. 13. As this rain area moved over UW during the period labeled "period 2" in Fig. 11, the raingage trace showed several peaks of heavy rainfall, each 1–3 min in duration, indicating that the small mesoscale rain area contained cumulus-scale convection (consisting of cells ~1 km in horizontal dimension). Since the radar data in Fig. 11 were averaged over 3 min periods, they probably do not fully resolve the embedded convection; however, the radar data for period 2 do show relatively short periods of enhanced fallspeeds which were not present before or after period 2. This is especially notable above the melting layer, where the velocity field was uniform during period 1 and quite variable during period 2. In Fig. 12, it can be seen that band B_4 was similar to B_1 in exhibiting a relatively non-convective period (period 3) and a more convective period (period 4).

Surprisingly, the changeover to a horizontally fluctu-

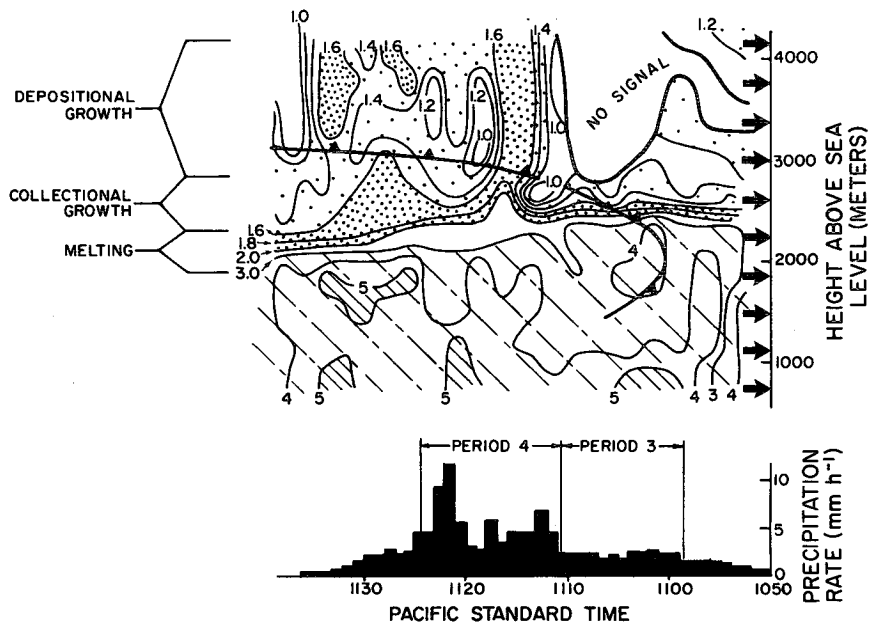

FIG. 12. As in Fig. 11 except for rainband B_4.

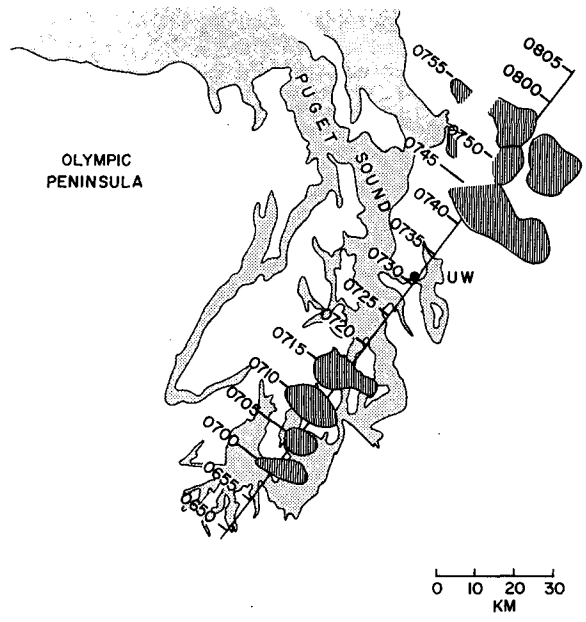

FIG. 13. Path of small mesoscale rain echo (cross hatched) seen on UW radar PPI on 20 December 1973. Times of interpolated echo positions are shown in the immediate vicinity of UW where the rain echo was obscured by ground clutter echoes.

ating pattern from period 1 to period 2 seen in Fig. 11 was not accompanied by any apparent change in particle growth modes. Above 2.8 km, the isotachs were oriented vertically during period 2, indicating that the dominant particle growth mode at these heights was deposition during, as well as before, period 2. The short periods of enhanced fall velocities in the snow region seen during period 2 apparently arose due to enhanced growth of particles in small-scale convective regions *above* the 4 km level. Particles from these growth regions then grew very little as they settled downward through the depositional growth region (located between 4 and 2.8 km in Figs. 11 and 12).

The existence of convective cells just above 4 km would be fully expected in bands B_1 and B_4 since potentially unstable air, seen near 650 mb (or 3.6 km) between 0600 and 1200 PST on 20 December in Fig. 3c, was being lifted to saturation by the airflow depicted in Fig. 8. The relative humidity pattern in Fig. 3b suggests that the tops of the convective cells (which had bases at about the 4 km level) were near the 5 km level.

Shallow convective cells located aloft in the snow regions of extratropical storms are a fairly common phenomenon. They have been described and referred to as "generating cells" by Marshall (1953). Browning and Harrold (1969) inferred the presence of such cells in warm frontal rainbands, and Austin and Houze (1972) noted cells of similar dimensions situated aloft in New England cyclones. Our study indicates that the microphysical growth of the precipitation particles in rainbands may be enhanced within these cells.

e. Ice particle types

Information on ice particle types can be inferred from the vertically pointing Doppler radar using a method developed in our group (Weiss *et al.*, 1976). This method is based on the assumption [supported by the results of Ohtake (1969)] that very little breakup of precipitation particles occurs within the melting layer. In this case, the power-weighted mass spectrum (that is, the spectrum of power returned to the Doppler radar expressed as a function of particle mass) should be the same for radar signals returned from just above and just below the melting layer (assuming that ice particles reflect electromagnetic radiation as if they were melted spheres of liquid water and that the width of the melting layer is small enough that range effects can be ignored).

The power spectrum $P(V)$ of particle fall velocity measured with the radar can be converted to the power-weighted mass spectrum $P(M)$ if there is a known one-to-one relationship between the particle mass M and velocity V. For raindrops such a relationship exists (e.g., Fletcher, 1962, pp. 194–195). However, for ice particles, V depends on the particle type as well as its mass, i.e.,

$$V = aM^b, \tag{2}$$

where a and b take on different values for different ice crystal types (see Locatelli and Hobbs, 1974). If the measured power spectrum of velocity *above* the melting layer is converted to a spectrum of mass $P_A(M)$ using (2), the resulting spectrum should match the power spectrum $P_B(M)$ of raindrop mass determined for the region just *below* the melting layer, provided the proper values of a and b are used in (2). The dominant crystal type can thus be inferred indirectly, by finding the combination of a and b which give the closest match between $P_A(M)$ and $P_B(M)$.

In Fig. 14, power spectra from above and below the

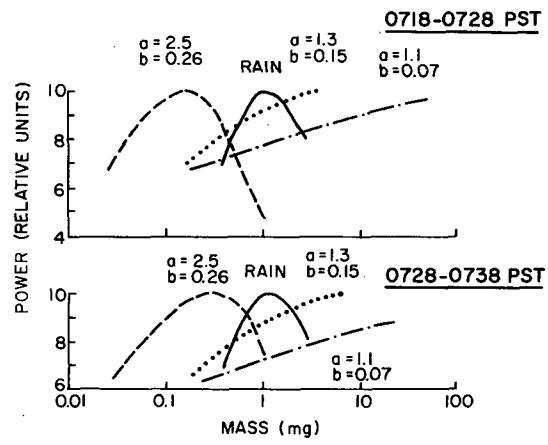

FIG. 14. Power-weighted mass spectra computed from Doppler radar data. Combinations of a and b are for different crystal types. Further explanation is given in text.

melting layer are compared for periods 1 and 2 within rainband B_1. The velocity spectra above the melting layer were converted to mass spectra using values of a and b for three types of ice particles, using the data of Locatelli and Hobbs (1974). Unfortunately, a close match with the raindrop spectrum was not obtained for any of these particle types. However, the *relative positions* of the snow and rain spectra did not change from period 1 to period 2, indicating that whatever the ice particle types were just above the melting layer, they were the same in the two periods. Moreover, the period 2 curves were shifted along the abscissa in Fig. 14 toward slightly higher particle masses, probably as a result of the enhanced particle growth in convective cells aloft during this period. We conclude, therefore, that the role of the cumulus cells was to increase the average particle masses and fallspeeds but not to change the fundamental crystal types.

f. Confirmation of radar results by direct aircraft sampling of rainbands

Fig. 15 contains vertical cross sections through rainbands B_3 and B_4 showing the data collected from the aircraft. On both the outbound (Fig. 15a) and inbound (Fig. 15b) flight legs, the continuous cloud liquid water content and turbulence measurements made aboard the aircraft showed no significant variations while the aircraft was within bands B_3 or B_4. In fact, the values of these variables were lower in rainbands B_3 and B_4 than in the tops of the low-level, non-precipitating stratocumulus clouds encountered by the aircraft between 1110 and 1130 PST (Fig. 5a) after it passed through the back edge of B_4 behind the cold front. The lack of any large or highly variable values of liquid water content or turbulence in the rainbands indicates an absence of convective activity at the flight level of the aircraft. This result is consistent with the Doppler radar and rawinsonde data which indicated that convective cells in the rainbands were located at altitudes of 4–5 km which were above the aircraft flight level.

By comparing Fig. 15 with Figs. 12 and 13, it can be seen that the flight level of the aircraft was within, but near the top of, the collectional growth region inferred from the Doppler radar data. We therefore expect the ice particles sampled by the aircraft to exhibit characteristics of growth by aggregation or riming. Generally, the ice particles sampled along the aircraft flight path were rather irregular and difficult to characterize. However, the few which could be identified were needles and sheaths. Evidence of smashed aggregates of crystals were noted in both Formvar and foil sample replicas, indicating that aggregation was a factor in precipitation growth. The probability that riming was also a factor in particle growth is indicated by the presence of both liquid water and ice along the flight path (Fig. 15). It is known that rimed crystals are most likely to consist of frozen droplets 15–45 μm in diameter and crystals larger than about 0.3 mm in dimension (Hobbs, 1974). From Fig. 15 it can be seen that the solid precipitation particles in rainbands B_3 and B_4 were 0.3–4 mm in dimension and drops 8–60 μm in diameter were present in concentrations of about 50 cm^{-3} on average. The smashed and amorphous nature of the sampled ice particles made it difficult to discern the degree to which particles were rimed.

g. Concentration of ice particles in the rainbands

The measured concentrations C of ice particles in rainbands B_3 and B_4 were in the range of 10–200 ℓ^{-1} (Fig. 15). At the cloud top temperature of -14°C which was typical of these bands (estimated from the relative humidity cross section in Fig. 3c), the active ice nucleus concentrations N should have been about $10^{-1.5}$ (Fletcher, 1962). The ratio C/N was therefore $10^{1.5}$ to $10^{3.8}$, indicating that ice enhancement was probably occurring in these bands. If the ice particles were actually nucleated below cloud top, i.e., at temperatures above -14°C, fewer ice nuclei would have been available for activation and the ice enhancement ratios would have been even greater than those given above. Hobbs and Atkinson (1976) have shown that ice enhancement is common in cyclonic storms over the Cascade Mountains, which lie just to the east of the region where the present measurements were made.

Recent laboratory experiments (Mossop, 1976) suggest that large numbers of secondary ice particles may be produced in clouds during riming if (i) the cloud temperature is between -3 and -8°C, (ii) cloud droplets >24 μm in diameter are present, (iii) the liquid water content is about 1 g m^{-3}, and (iv) the fallspeeds of the ice particles are between about 1 and 3 m s^{-1}. Although these laboratory results must be treated with caution at the present time, we note that the aircraft and Doppler radar measurements obtained in the present case study show that Mossop's criteria were closely met in rainbands B_3 and B_4. It is therefore possible that the observed high ice particle concentrations in those bands were produced by ice multiplication during riming.

10. Conclusions

This study has advanced our understanding of the mesoscale structure of extratropical cyclones in the direction of a better physical understanding of the rainbands. The measurements obtained in the CYCLES PROJECT cover a sufficiently wide range of scales (from the synoptic scale down to the cloud particle scale) to permit an examination of the dynamical framework in which the bands exist and the detailed microphysical processes which are at work within the rainbands themselves.

In the case study presented here, we have examined the dynamical and microphysical processes associated

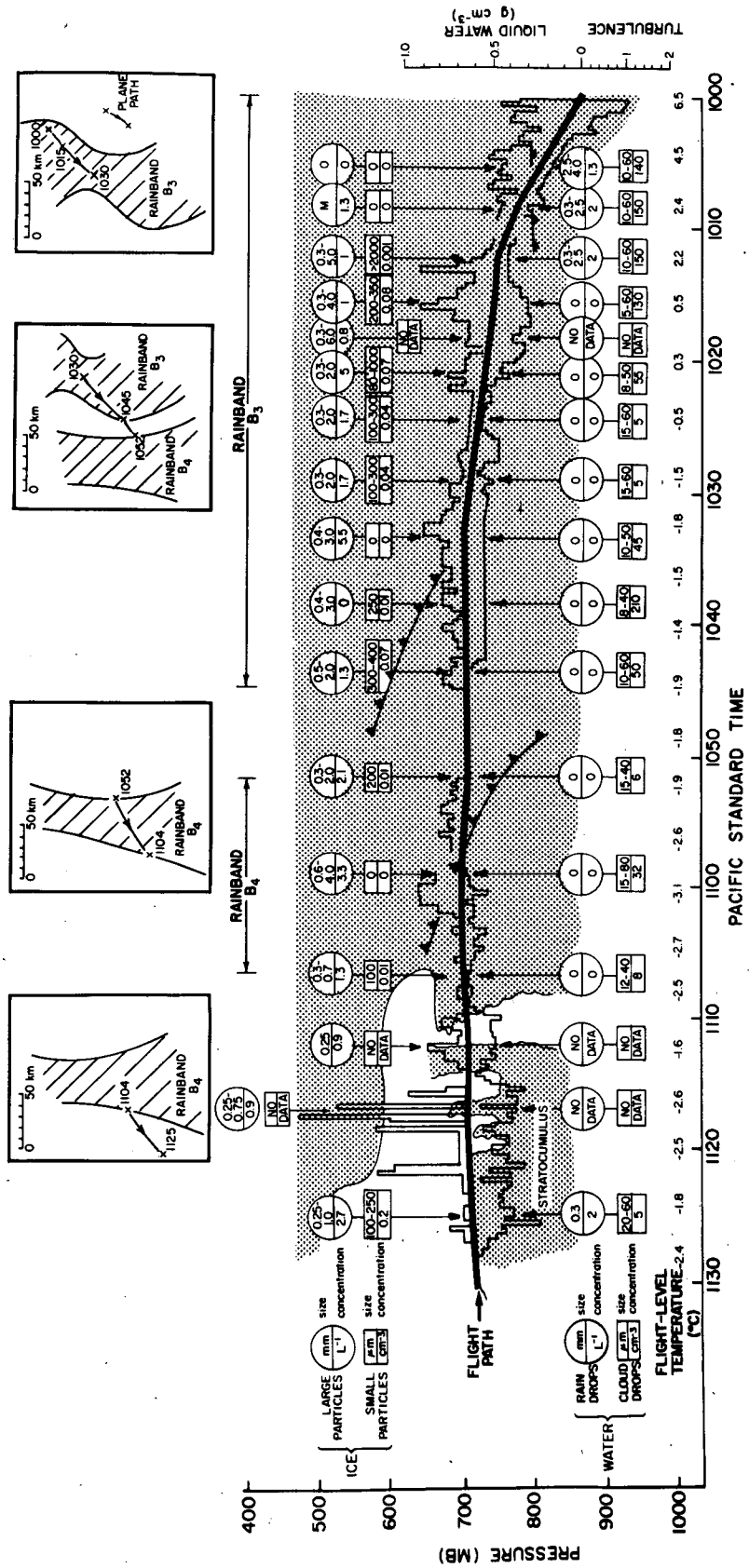

FIG. 15. Vertical cross sections showing aircraft measurements obtained in clouds associated with rainbands B_3 and B_4. The inset drawings in (a) and the inset on the left in (b) show plan views of the aircraft's flight path in relation to rainbands. In (b) the three insets on the right show the aircraft's flight path in relation to radar echoes of intense cores of precipitation embedded in rainband B_4. In the vertical cross sections, shaded areas indicate cloudy regions. The origins of the turbulence and liquid water content plots are centered on the flight path line. Whereas turbulence and liquid water content were measured continually during the flight, ice particle and drop sizes and concentrations (indicated in circles and boxes) were determined only at discrete intervals by replication sampling. The letter M indicates particles were melting and therefore could not be accurately sized.

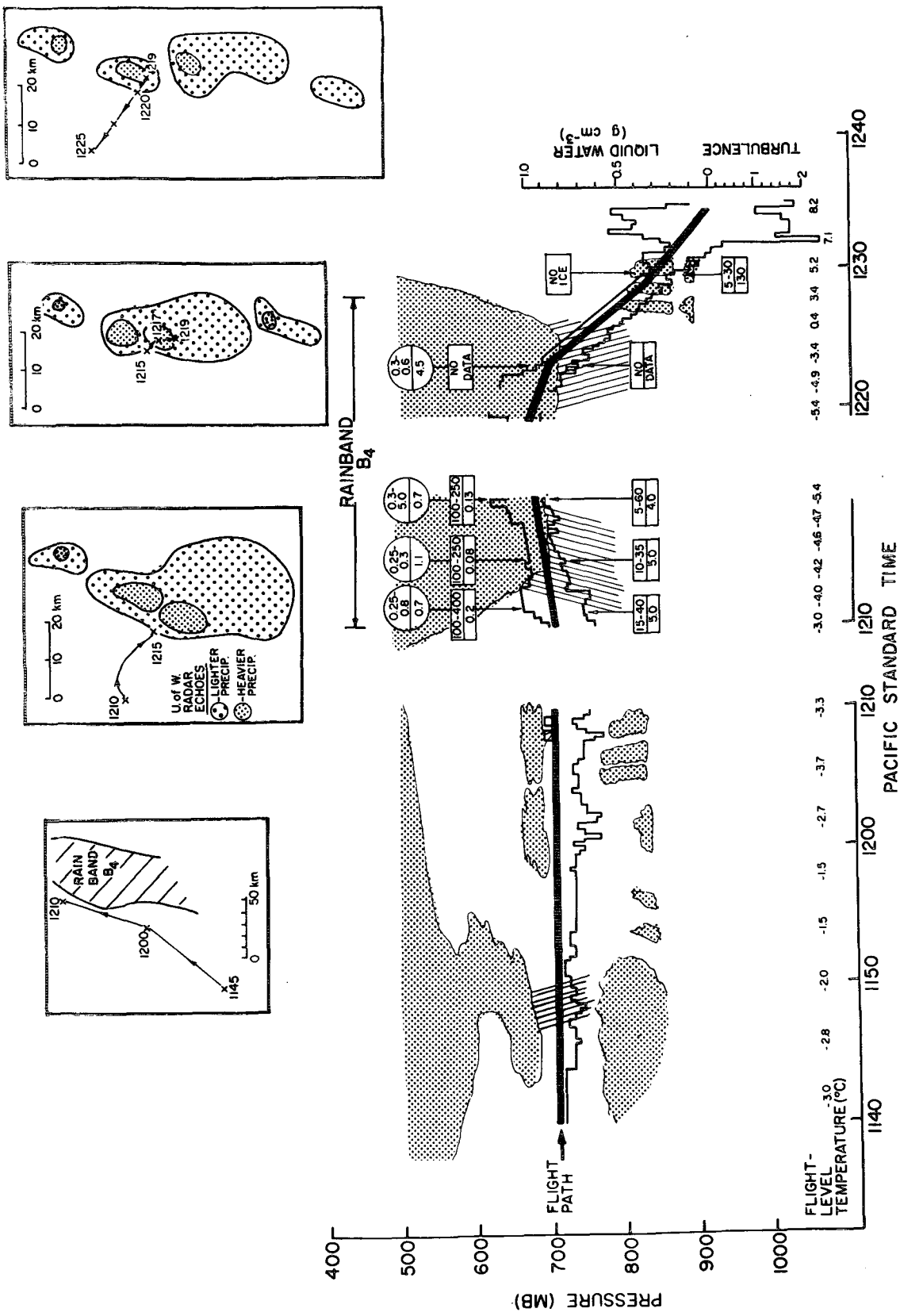

(b)

FIG. 15. (*continued*)

with four rainbands in an occluded cyclone. The principal conclusions we have arrived at are as follows:

1) Two rainbands oriented parallel to the warm front of the occlusion were located in the leading portion of the frontal cloud shield, while two rainbands with cold frontal orientations were observed in the trailing portion of the frontal system.

2) Mesoscale features in the surface pressure field appeared to be parallel to the rainbands as they moved onshore from the Pacific Ocean; however, as one of those pressure features moved inland toward the Cascade Mountains, it lost its parallel relationship to the rainbands.

3) Two- and three-dimensional airflow patterns, constructed using vertical velocities computed two-dimensionally from serial rawinsonde data, were in good agreement with observed cloud and precipitation patterns.

4) The computed airflow patterns indicated that the rainbands were supplied with moist air which entered the cloudy region at very low levels (below 800 mb and below the warm front) and rose abruptly in the region of the rainbands as the moist air flowing into the frontal system from the south to south-southwest was overtaken by the eastward moving frontal system.

5) Cumulus convection (or "generating cells") apparently existed within the rainbands in a shallow layer aloft (between 4 and 5 km). The convective cells increased the growth of ice particles aloft but did not have any apparent effect on crystal habits.

6) Below the base of the convective layer, ice particles in the rainbands drifted downward, growing at first by vapor deposition, then, beginning at about the 2.8 km level, by riming or aggregation.

7) Direct aircraft sampling of the cloud and precipitation particles indicated that ice enhancement was occurring in the rainbands.

8) Below the melting layer little growth of raindrops occurred, and in the two warm frontal rainbands considerable evaporation of raindrops was observed at low levels.

While this study represents an important step toward understanding the dynamics and microphysics of rainbands, much work remains to be done. Case studies of the type reported here can be improved greatly by multi-level aircraft sampling. Weather radars should be used in real time to identify and monitor the rainbands and direct the research aircraft into different levels of the bands. Studies of this type are now under way as part of the CYCLES PROJECT.

Acknowledgments. We wish to thank all members of the University of Washington Cloud Physics Group who helped in this study. Special thanks go to Dr. R. R. Weiss and Dr. L. R. Radke for managing the radar and aircraft observations, respectively.

This research was supported by the Atmospheric Research Section (Meteorology Program) of the National Science Foundation and by Contract F19 628-74-C-0066 from Air Force Cambridge Research Laboratories.

REFERENCES

Austin, P. M., and R. A. Houze, Jr., 1972: Analysis of the structure of precipitation patterns in New England. *J. Appl. Meteor.*, **11**, 926–935.

Browning, K. A., 1974: Mesoscale structure of rain systems in the British Isles. *J. Meteor. Soc. Japan*, **50**, 314–327.

——, and T. W. Harrold, 1969: Air motion and precipitation growth in a wave depression. *Quart. J. Roy. Meteor. Soc.*, **95**, 288–309.

——, M. E. Hardman, T. W. Harrold and C. W. Pardoe, 1973: The structure of rainbands within a mid-latitude depression. *Quart. J. Roy. Meteor. Soc.*, **99**, 215–231.

Elliott, R. D., and E. L. Hovind, 1965: Heat, water and vorticity balance in frontal zones. *J. Appl. Meteor.*, **4**, 196–211.

Fletcher, N. H., 1962: *The Physics of Rainclouds.* Cambridge University Press, 390 pp.

Harrold, T. W., and P. M. Austin, 1974: The structure of precipitation systems—a review. *J. Rech. Atmos.*, **8**, 41–57.

Hobbs, P. V., 1974: *Ice Physics.* Oxford University Press, 837 pp.

——, and D. G. Atkinson, 1976: The concentrations of ice particles in orographic clouds and cyclonic storms over the Cascade Mountains. *J. Atmos. Sci.*, **33**, 1362–1374.

——, R. A. Houze, Jr., and T. J. Matejka, 1975: The dynamical and microphysical structure of an occluded frontal system and its modification by orography. *J. Atmos. Sci.*, **32**, 1542–1562.

Houze, R. A., Jr., P. V. Hobbs, K. R. Biswas and W. M. Davis, 1976: Mesoscale rainbands in extratropical cyclones. *Mon. Wea. Rev.*, **104**, 868–878.

Kreitzberg, C. W., 1964: The structure of occlusions as determined from serial ascents and vertically-directed radar. Res. Rept. AFCRL-64-26, University of Washington, 121 pp. [Available from Air Force Cambridge Research Laboratories, L. G. Hanscom Field, Mass.]

——, and H. A. Brown, 1970: Mesoscale weather systems within an occlusion. *J. Appl. Meteor.*, **9**, 417–432.

Locatelli, J. D., and P. V. Hobbs, 1974: Fallspeeds and masses of solid precipitation particles. *J. Geophys. Res.*, **79**, 2185–2197.

Marshall, J. S., 1953: Precipitation trajectories and patterns. *J. Meteor.*, **10**, 25–29.

Mossop, S. C., 1976: Production of secondary ice particles during the growth of graupel by riming. *Quart. J. Roy. Meteor. Soc.*, **102**, 45–56.

Ohtake, T., 1969: Observations of size distributions of hydrometeors through the melting layer. *J. Atmos. Sci.*, **26**, 545–557.

Weiss, R. R., and P. V. Hobbs, 1975: The use of a vertically pointing pulsed Doppler radar in cloud physics and weather modification studies. *J. Appl. Meteor.*, **14**, 222–231.

——, J. D. Locatelli and P. V. Hobbs, 1976: Preliminary explorations of a technique for deducing ice crystal habits and growth modes from Doppler radar measurements. *Preprints 17th Radar Meteorology Conf.*, Seattle, Amer. Meteor. Soc., 226–227.